Mongold, E., Baker, J.W. (2025). "Quantifying Climate Change Risk through Natural Hazard Losses to Inform Adaptation Action." *Climatic Change* 178, 82.
https://doi.org/10.1007/s10584-025-03927-2

Quantifying Climate Change Risk through Natural Hazard Losses to Inform Adaptation Action

Emily Mongold[1*] and Jack W. Baker[1]

[1]Civil and Environmental Engineering Department, Stanford University, Panama Mall, Stanford, 94305, CA, USA.

*Corresponding author(s). E-mail(s): emongold@stanford.edu;

Abstract

Climate change is expected to increase the frequency and severity of many natural hazards. In particular, coastal communities are often exposed to multiple hazards, exacerbated by climate change. We present a methodology to quantify the increase in multi-hazard risk due to climate change. The methodology includes a probabilistic description of independent hazard pathways, defined as sets of individual and cascading hazards that are statistically independent, run for multiple levels of climate change impact. We also quantify the risk reduction from adaptation actions. The approach integrates probabilistic hazard analysis and loss assessment. With this approach, we identify the hazards contributing most to risk under multiple amounts of climate change. This methodology is applied to a case study of residential housing in Alameda, California, USA, considering how sea level rise impacts multiple hazards: earthquakes, coastal flooding, and tsunamis. For the case study location, we identify that the highest annualized risk shifts from earthquakes to coastal flooding as sea levels rise. We assess how different adaptation actions would reduce the risk today and under sea level rise, highlighting the need to consider frequent and infrequent losses.

1 Introduction

Coastal communities are already seeing the impacts of climate change. As sea levels and temperatures rise, so do the frequency and intensity of coastal hazards. Many individual hazards are intensifying, including flooding (Hadipour et al., 2020; Buchanan et al., 2016), hurricanes (Mousavi et al., 2011; Shepard et al., 2012), tsunamis (Alhamid et al., 2022; Dura et al., 2021; Li et al., 2018; Sepúlveda et al., 2021), coastal erosion (Leatherman et al., 2000; Gornitz, 1991), rising and emergent groundwater (Befus et al., 2020; Bosserelle et al., 2022), and resulting increases in liquefaction induced by earthquakes (Grant et al., 2021). This body of work serves to understand how the intensity of hazards are anticipated to

increase in the coming decades.

Risk analysis is a useful tool to quantify how coastal communities will be affected by increases in natural hazards. According to the IPCC, risk is the "potential for adverse consequences for human or ecological systems" (Reisinger et al., 2023). In a risk analysis context, risk is the combination of a hazard, the event that can cause damage; the exposure, or the assets that may incur damage; and the vulnerability, or the likelihood and extent of damage that may be incurred. While definitions of risk have varied in previous literature, this work uses the IPCC definition of risk throughout.

Risk analyses are often based on probabilistic analyses of individual hazards (e.g. Hadipour et al., 2020). This framework allows for incorporating underlying uncertainty and utilizing event sets that contain an array of possible hazard scenarios. Beginning with probabilistic seismic hazard analysis (e.g. Cornell, 1968), this method has been adapted to many hazards, such as probabilistic tsunami hazard analysis (e.g. Park et al., 2018). Flooding typically uses generalized extreme value and peaks over thresholds, though there are many ways to make flood hazard maps, including physical or empirical modeling (e.g. Morrison and Smith, 2002). These analyses are a useful basis of risk analysis, but often neglect interactions and underestimate the risk to an area that faces more than one hazard.

In the context of a community, multi-hazard risk is the total risk to an asset of interest from any hazard. Property owners, residents, and local governments are affected by loss of property, lives, and functioning regardless of the cause. While much work has gone into the qualitative classification of multi-hazard interactions, sparse quantitative studies do not cover the full hazard space (Gill and Malamud, 2014; Opabola, 2024). Some frameworks focus on cascading hazards alone, such as earthquake triggering tsunami, earthquake triggering landslide, or flood triggering landslide (e.g. Sanderson et al., 2022; Dunant et al., 2025; Kwag et al., 2019; Zhang and Zhang, 2017). Many current frameworks work toward hazard coincidence modeling, though these are mostly limited to hypothetical or idealized studies (Opabola, 2024; Iannacone et al., 2024; Schlumberger et al., 2024; De Angeli et al., 2022; Otárola et al., 2024), or limited to a specific hazard coincidence scenario (e.g. Ming et al., 2015). These studies tend to be limited to two interacting hazards, due in part to computational limitations (Selva, 2013). Some studies consider spatial overlap of single-hazard risk, termed multilayer single hazard by Gill and Malamud (2014). These studies are often semi-qualitative, with risk indices (Kappes et al., 2012), and on an aggregate scale, whether regional, national, or global (e.g. Boruff et al., 2005; Lung et al., 2013; Forzieri et al., 2016; Skilodimou et al., 2019; Ballesteros and Esteves, 2021). Most similar to the present study, Bell and Glade (2012) calculate multi-hazard risk in terms of loss of life from three hazards which are assumed to be independent; while quantitative in nature, the framework is not readily transferable to include cascading events or formalized for application in different multi-hazard environments.

Efforts to include future climate conditions in hazard risk have focused on a single hazard (Laurien et al., 2022), especially hazards most impacted by changing climate, such as temperature, wind, rain, and flood (e.g. Vlachogiannis et al., 2022; Smits et al., 2024; Alhamid

et al., 2022). However, as hazards are still commonly studied in isolation, direct comparisons between risk in present and future climate are not available. Kafi et al. (2024) highlight a need for more risk prediction and mitigation studies focusing on the category of weather and climate extreme events. The gap remains for a probabilistic, multi-hazard risk assessment that quantifies climate risk as the change in multi-hazard risk under climate change.

Multi-hazard frameworks also serve to inform adaptation actions. There are many potential trade-offs between actions for different hazards, such as raised houses for flood protection being more vulnerable to ground shaking in an earthquake (Goldwyn et al., 2021). Few past works have considered interactions of hazards and vulnerability (Kappes et al., 2012), many of which are necessary to include overlapping or coincident hazards in risk analysis and adaptation action assessment. Past studies have considered adaptation and protection costs, including retreat, seawall, and beach nourishment (Leatherman, 2001). Another study on small island developing states considers hard protection, nature-based solutions, retreat, and early warning (Martyr-Koller et al., 2021). The Coastal Impact and Adaptation Model finds that retreat is more effective than protection for the majority of global coastlines, with a large benefit of adaptation overall, and determines the populated locations where protection is preferable to retreat (Diaz, 2016). Updated models and data show that while the majority of coastlines should be retreated, the majority of population (80%) is located on coastlines that have a higher cost-benefit from the protection strategy, though this is noted to be sensitive to a change in the retreat cost parameter (Depsky et al., 2023). All of these studies are at large scales, and relatively qualitative in their recommendations, with broad categories of risk and limited quantitative assessment. The question remains on a local level of how to consider the cost and trade-offs of different adaptation actions, especially considering multiple hazards.

Sea level rise (SLR) risk has also been quantified from an economic perspective. Literature on SLR impacts is largely focused on coastal flooding or inundation without considering storm events (e.g. Al-Mutairi et al., 2021). The economic loss studies have considered land loss (Anthoff et al., 2010), depreciated land value (Diaz, 2016), land use (Prime et al., 2015), indirect costs through impact on industries and GDP (Turner et al., 1995; Bosello et al., 2012), and social vulnerability or people affected (Bosello et al., 2012; Felsenstein and Lichter, 2014; Martyr-Koller et al., 2021). These studies are mostly on a country or global scale (Darwin and Tol, 2001; Leatherman, 2001; Anthoff et al., 2010; Diaz, 2016). While these studies are useful for large-scale economics, they do not translate down to household- or individual-level impacts.

Multiple hazards can combine in various ways, physically and probabilistically, and those relationships have been defined in many ways in the literature (e.g. Liu et al., 2016; Tilloy et al., 2019; Zscheischler et al., 2020). In this work, a multi-hazard analysis refers to a workflow that probabilistically combines multiple individual hazards in an area. Cascading events are secondary hazards caused by an initial triggering event. Each cascading event, such as earthquake-induced liquefaction, has a probability of occurrence conditioned on the triggering event occurring.

This paper addresses the highlighted gaps of asset-level multi-hazard risk analysis on a community scale. We include multiple probabilistic hazards under climate change through a risk analysis framework. This framework is general and can be applied to multiple climate change measures and multiple downstream impacts on humans and the built environment. We quantify climate risk as the increase in natural hazard risk between present-day and future climate conditions. The framework can be used to identify the largest sources of risk today and in future climates. We apply this framework to a case study of Alameda, CA, USA to quantify sea level rise risk. Alameda is subjected to earthquake, coastal flooding, and tsunami hazards. We find that Alameda's primary risk is shifting from earthquake to coastal flooding. Finally, we compare adaptation actions by their reduction in risk, showing trade-offs between frequent and rare losses.

2 Methodology

Fig. 1 presents a general methodological overview. First, choose a location for study and identify assets of interest that will be assessed, such as roadways, critical infrastructure, buildings, or human life. Next, identify hazards that are relevant for both the location and assets of interest. Some combinations of hazard and asset are not necessary to consider. For example, heatwaves may be important for human health impacts or agriculture, but would not damage buildings. Thus, the hazards chosen are informed by both the area of interest and the assets of interest.

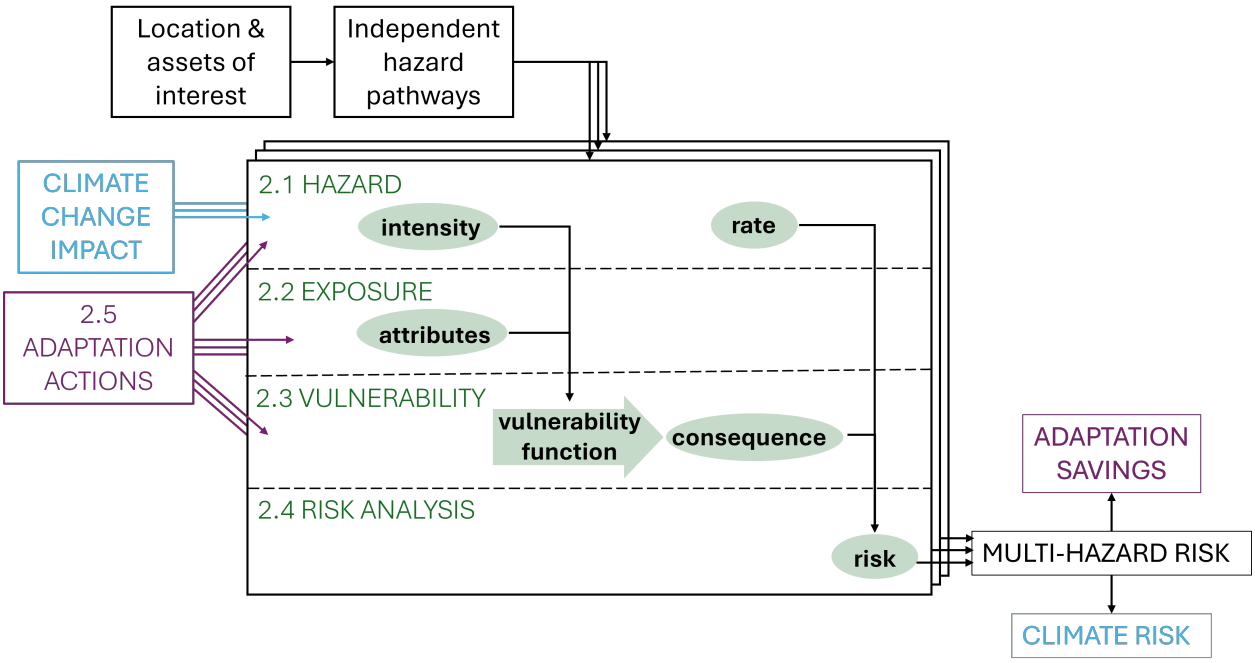

Fig. 1 Overview of the methodology for multi-hazard risk assessment under climate change. The three large stacked panes denote multiple hazard pathways, ellipses denote intermediate metrics within each hazard pathway, the arrow shape denotes a function within each hazard pathway, and rectangles denote multi-hazard attributes. Numbers indicate section numbers where aspects of the methodology are discussed in more detail.

Once we identify relevant hazards, we separate them into independent hazard pathways. Independent hazard pathways are statistically independent combinations of hazards (with associated cascading events), containing a probabilistic characterization of each hazard. We define independent hazard pathways to synthesize qualitative multi-hazard works that connect hazards through triggering and changing probabilities of additional hazards (e.g. Gill and Malamud, 2014). In this framework, one hazard may be represented in multiple pathways. For example, a location may have near-field and far-field tsunami hazards from different faults. The near-field tsunami would be represented as a cascading hazard from an earthquake, all in one independent hazard pathway. However, the far-field tsunami, generated from seismic hazard not captured within the area of interest, would be its own independent hazard pathway causing inundation alone.

For the next step shown in Fig. 1, hazard and risk analyses are performed in parallel for each independent hazard pathway. This analysis includes the simulation of relevant information about hazard, exposure, vulnerability, and risk. Hazard intensity and attributes of the exposure feed into the vulnerability function, which returns a consequence. The hazard rate and consequence together inform the risk. The interactions between hazard, exposure, and vulnerability parameters highlight the need to select these data in concert. The relationships within an independent hazard pathway may be more complex depending on the specific hazards included in that pathway and the number of cascading events.

The risk metrics from each of the independent hazard pathways are combined to quantify the output multi-hazard risk. The entire simulation process is repeated for future climate change amounts. As represented in Fig. 1, the climate change impact affects the hazard portion of the analysis and outputs the climate risk from the multi-hazard risk metric. In addition, the whole process is repeated under adaptation actions, which can affect hazard, exposure, and/or vulnerability. The adaptation analysis quantifies potential adaptation savings from the multi-hazard risk.

This methodology is generalizable to other hazards, exposed assets, and climate risk metrics. For example, any hazards that affect an area can be separated into independent hazard pathways. Following the qualitative framework of Gill and Malamud (2014), cascading hazards can be classified probabilistically following a primary event, in a chain of many hazards, at times. Using this framework, the secondary hazard will have an increased probability from its baseline. Hazards such as landslides may be repeated in multiple independent hazard pathways such as flood or earthquake, which are independent triggers. In addition, multiple types of assets can be considered. Residential buildings have a simple relationship on a community scale, while networks such as roadways or power systems have a more complex total consequence than a summation of component damage costs. Given the relevant vulnerability data, an output risk metric can be defined for any exposed assets of interest. Finally, changes in hazards can be driven by factors beyond sea level rise, such as concentrations of greenhouse gases, or changes in ocean or land temperature. The climate change metric will depend largely on the availability of hazard models under these changes, and the consequences of interest. For example, if human health impacts of wildfire smoke are of interest, temperature and other atmospheric metrics can be used to quantify the changing hazard.

2.1 Hazard

The hazard data are regional-scale probabilistic hazard scenarios. These scenarios cover the region of interest and have associated rates and intensities. The hazard includes an intensity measure, IM, and occurrence rate, λ. One pathway may consist of multiple intensity measures related to multiple phenomena or multiple features of the hazard. In addition, multiple IMs may be used to describe the hazard, either a single hazard or including cascading effects.

Initially, a baseline analysis is run for present-day conditions. Then, the whole analysis is re-run under multiple future climate conditions. Future climate conditions will be reflected by changes in the hazard model. If hazard models are available under these future climate conditions, they can be applied directly. If models for future climate conditions are not available for some hazards, some assumption needs to be made about the change in that hazard. For example, for liquefaction hazard, the change due to sea level rise comes from a change in the depth to groundwater.

2.2 Exposure

The exposure data contains information about the assets of interest. These assets may be a part of the built environment or population, such as houses, roadways, agriculture, or people. Each asset has a location and attributes. The attributes are informed by the specific asset as well as by the vulnerability relationships that are available, as discussed in the next section. Some examples of necessary attributes may be the dollar value, the number of stories in a building, the length of a roadway, or demographic information about people. Necessary exposure attributes depend on the asset of interest, expected impacts from the natural hazards, and vulnerability function. For example, for flooding, the presence of a basement may be important, whereas for wildfire, the exterior cladding material may be more relevant.

The exposure data is ideally available at the asset level. However, attributes can be approximated from larger-scale aggregated data. This method will produce accurate results aggregated at the level of initial data, but is not precise at the asset level. One example is to approximate the structural types of buildings from Hazus tables (FEMA, 2002), or to infer resident demographic characteristics from neighborhood or city-level data.

2.3 Vulnerability

The vulnerability data characterize the susceptibility of assets to damage or another output consequence metric of interest, when subjected to hazard scenarios. This step typically utilizes a vulnerability function that inputs hazard intensity and outputs a consequence metric. This consequence metric is often damage, but can be many other metrics. The vulnerability function is defined as

$$C = f_{i,k}(IM) \tag{1}$$

where the consequence metric, C, is a function of the hazard intensity measure, IM. The function depends on attributes of the asset, k. Each hazard pathway, i, has a different vulnerability function as they are measured by a different IM and may cause different

amounts of impact. Thus, the vulnerability specification requires information for each of the hazards and assets considered in the analysis. In cases where cascading hazards exist, the vulnerability functions should account for collective impacts from all hazards. This may be a complex function that accounts for a vector of IMs from the primary and cascading hazards.

2.4 Risk analysis

Risk analysis determines the potential consequences of hazards on humans and the built environment. The average annual value of the consequence metric, AAC, for a given hazard pathway, i, at a specific asset, k, is defined as

$$AAC_{i,k} = \sum_{j=1}^{n_{scen,i}} C_{i,j,k} \cdot \lambda_{i,j} \tag{2}$$

where j is the scenario from 1 to the total number of scenarios, $n_{scen,i}$, for a given hazard pathway, i. The consequence, C, of interest is defined for a specific hazard pathway, i, scenario, j, and asset, k. The occurrence rate for each pathway and scenario is $\lambda_{i,j}$.

One limitation of the current framework is that coincidence of events from independent hazard pathways is ignored. In combination with work that focuses on hazard coincidence, this framework could be applied to consider event occurrence over time and capture the frequency of coincidence. At present, neglecting coincidence of rare events is not expected to contribute largely to total risk; however, as events become more frequent under climate change, this limitation will have a larger impact.

At a community level, the consequence metric will be a function of individual asset C_k. For some assets, the community C will be a summation of asset C_k, however, for other interconnected systems, this function will be more complex. For example, damage to power infrastructure may be measured by damages at the individual asset level, but the downstream community metric of access to power will depend on the specific system function.

Community-level $C_{i,j}$ is a function of the asset-level consequence metric, $f(\{C_{i,j,k} \mid k \in n_{asset}\})$ where $\{\cdot\}$ indicates the set of values for every asset in the inventory, n_{asset}. $[\cdot]$ is the indicator function, equal to 1 if true and 0 if false. Thus, the summation over all scenarios will include the rate of each event that produces a $C_{i,j}$ exceeding the threshold, C. This value is summed over all hazards, n_{hazard}, and all scenarios, $n_{scen,i}$. Additionally, at the community level, the average annual consequence metric is defined as

$$AAC_{total} = \sum_{i=1}^{n_{hazard}} \sum_{j=1}^{n_{scen,i}} C_{i,j} \cdot \lambda_{i,j} \tag{3}$$

where *total* indicates that all hazards are included. The AAC_i can also be calculated for each independent hazard pathway, i, so that the portion of AAC attributed to each hazard pathway can be calculated as

$$AAC_{norm,i} = \frac{AAC_i}{AAC_{total}} \tag{4}$$

where the normalized value can be calculated for the entire community. Using the same formulation at the asset level, $\frac{AAC_{i,k}}{AAC_{total,i,k}}$, gives the normalized contribution to annualized

risk from each individual hazard at an asset level, $AAC_{norm,i,k}$. This risk metric indicates the portion of risk attributed to each hazard on the community and individual building level, which can be used to guide intervention policies.

To calculate climate change risk, the analysis is re-run under future climate conditions, either for amounts of SLR or global mean temperature increase. Then, the change in hazard risk between the present-day baseline and the future climate condition is attributable to that aspect of climate change. Thus, the annualized climate change risk metric is defined as

$$\Delta AAC_x = AAC_x - AAC_0 \tag{5}$$

where x is a particular measure of climate change impact, for example, degrees of warming or meters of SLR, and AAC_0 is the present-day average annual consequence metric. Δ signifies the change, so ΔAAC_x is the change in the average annual consequence metric at x amount of climate change impact.

An exceedance curve can be constructed with the annual rates of exceedance, λ_c, for given values of the consequence metric, c, at the community level. This rate is calculated as

$$\lambda_c = \sum_{i=1}^{n_{hazard}} \sum_{j=1}^{n_{scen,i}} [C_{i,j} > c] \cdot \lambda_{i,j} \tag{6}$$

where c is the threshold consequence metric value, and $C_{i,j}$ is the value for a given hazard pathway, i and scenario, j, at the community level.

2.5 Adaptation actions

The final step in this workflow is to determine the efficacy of adaptation actions to reduce natural hazard and climate risk. For this analysis, the first step is to identify potential adaptations to reduce risk. These actions can reduce any aspect of the risk: hazard, exposure, or vulnerability. For example, ground water level hazards could be reduced by pumping groundwater. Exposure could be reduced by raising buildings so that they are not as easily reached by flooding. Vulnerability could be reduced by retrofitting buildings so that they are stronger and less likely to be damaged by earthquake ground shaking.

The efficacy of adaptation actions is quantified via the reduction in annualized risk, which is the savings due to the adaptation at a given level of climate change impact, x, defined as

$$\Delta AAC_{x,adapt} = AAC_{total,x} - AAC_{total,x,adapt} \tag{7}$$

where the $AAC_{total,x}$ is the average annual consequence metric value for the entire asset portfolio at a given level of climate change impact, and $AAC_{total,x,adapt}$ is the same measure under an adaptation action.

The consequence threshold defined in Eqn. 6 can be defined as a function of exceedance rate, λ:

$$c(\lambda) = \min\{c \mid \lambda_c \leq \lambda\}. \tag{8}$$

where $c(\lambda)$ is the consequence value with an exceedance rate, λ_c, equal to or just below the exceedance rate of interest, λ.

The savings from an adaptation action can be quantified as the reduction in $c(\lambda)$ using the following equation,

$$\Delta c(\lambda) = c_x(\lambda) - c_{x,adapt}(\lambda) \tag{9}$$

where Δ indicates the change, $c_x(\lambda)$ is the consequence value at climate change impact, x, and $c_{x,adapt}(\lambda)$ is the corresponding consequence under the same climate impact under some adaptation action, *adapt*.

3 Case study

The case study of Alameda, CA, is set up as outlined in Section 2. Alameda is a low-lying and largely residential island with a population of 75,000 (Fig. 2). It is prone to coastal flooding, located near several active faults, and known to be susceptible to tsunami inundation from far-field sources. Additionally, the artificial fill soil, indicated in the lighter portion of Fig. 2, is highly susceptible to liquefaction during ground shaking. The climate impact we assess is sea level rise (SLR). While Alameda is exposed to pluvial (rainfall-induced) flooding, it is not a concern at present-day (City of Alameda, 2019) and climate projections have low agreement for precipitation in the San Francisco Bay region and show no clear trend of increasing rainfall with SLR (U.S. Geological Survey). Thus, we neglect pluvial flooding in this study, focusing on the risk from SLR specifically.

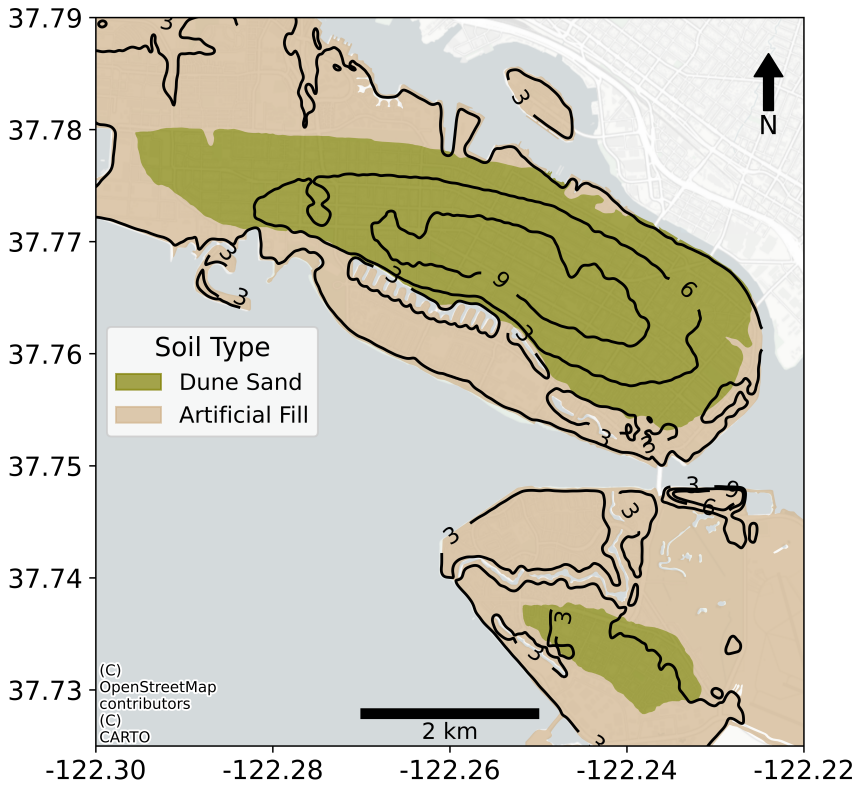

Fig. 2 Site map of Alameda, CA. Contours indicate smoothed 3m intervals of elevation from a mean sea level datum. Color represents the geologic deposit, whether artificial fill or dune sand. The soil deposit map is based on Witter et al. (2006).

Following through Fig. 1 to define case-study-specific details, the asset of interest here is residential housing. The three independent hazard pathways are earthquake, coastal flooding, and tsunami. Table 1 provides details for each element of the data and simulation. The details are provided for each of the independent hazard pathways. While coastal flooding and tsunami have the same intensity measure, water depth, they have different vulnerability functions that relate depth to damage. The exposure data necessary for each hazard also varies; while all hazards need the location of buildings, earthquake utilizes the structural type and year of construction and the water hazards require the number of stories. The climate risk that we quantify is SLR risk, repeating analysis for 0.25 m intervals from 0 - 1.5 m SLR. The considered adaptation actions include managed retreat, raising buildings, and seismic retrofit.

Table 1 Elements of each independent hazard pathway in the case study. Citations give the sources of data or equations. Adaptation actions lists which actions affect each independent hazard pathway.

	Earthquake	**Coastal flooding**	**Tsunami**
Intensity Measure	Peak ground acceleration (pga), liquefaction potential index (LPI)	Water depth (d)	Water depth (d)
Exposure	Location, construction year, structural type	Location, number of stories, first floor elevation	Location, number of stories, first floor elevation
Vulnerability function	FEMA (2020); Geyin and Maurer (2020)	Wing et al. (2020)	Suppasri et al. (2013)
Climate change impact	Depth to groundwater (Barnard et al., 2019)	Water depth (Vandever et al., 2017)	Water depth, see Supplementary Information
Adaptation actions	Retrofit, managed retreat	Raising houses, managed retreat	Raising houses, managed retreat

Table 2 maps consequence metrics from the Methodology to those specific to the case study. In general, the consequence of interest is loss ratio, LR, a unitless metric for the portion of building replacement value, BRV that is damaged. Loss is defined as the product of LR and BRV for each building. The community loss is the sum of losses over all residential buildings. The community loss metric does not consider indirect losses or any nonlinear effects of large total losses. Loss is measured in dollar values [USD]. The case study specific metrics will be used for the remainder of the paper.

3.1 Hazard

The earthquake hazard consists of two components: ground shaking and cascading ground failure, or liquefaction. Ground shaking intensity is measured in peak ground acceleration, pga, and simulated with the python package pypsha (Sharma, 2023). Earthquake occurrence

Table 2 Definitions of case-study-specific vulnerability and risk metrics related to each general vulnerability and risk metric as defined in the Methodology.

General Methodology		Case Study	
Metric	**Definition**	**Metric**	**Definition**
C	Consequence metric (Eqn. 1)	LR	Loss ratio
$AAC_{i,k}$	Average annual consequence (Eqn. 2)	$AALR_{i,k}$	Average annual loss ratio
AAC_{total}	Average annual consequence (Eqn. 3)	AAL_{total}	Average annual loss [USD]
$AAC_{norm,i}$	Portion of AAC from hazard i (Eqn. 4)	$AAL_{norm,i}$	Portion of AAL from hazard i
ΔAAC_x	Annualized climate change risk (Eqn. 5)	ΔAAL_x	Annualized sea level rise risk [USD]
λ_c	Annual rate of consequence exceedance (Eqn. 6)	λ_l	Annual rate of loss exceedance $[yr^{-1}]$
$\Delta AAC_{x,adapt}$	Adaptation reduction in AAC (Eqn. 7)	$\Delta AAL_{x,adapt}$	Adaptation savings of AAL [USD]
$c(\lambda)$	Consequence metric for a given exceedance rate (Eqn. 8)	$l(\lambda)$	Loss value for a given exceedance rate [USD]
$\Delta c_{x,adapt}(\lambda)$	Risk reduction due to adaptation (Eqn. 9)	$\Delta l_{x,adapt}(\lambda)$	Savings due to adaptation [USD]

rates are from the Uniform California Earthquake Rupture Forecast, Version 2 (Field et al., 2003). Three equally weighted ground motion models are considered (Abrahamson et al., 2014; Boore et al., 2014; Chiou and Youngs, 2014), and ground motion spatial correlations are included (Baker and Jayaram, 2008). This process outputs pga across the study area for 2423 simulated earthquake ruptures.

We use the liquefaction potential index (LPI) to quantify ground failure potential (Iwasaki et al., 1978). LPI is calculated from empirical equations that are functions of soil properties, ground shaking, and depth to groundwater. Two equally weighted equations are considered (Moss et al., 2006; Boulanger and Idriss, 2014). The soil properties depend on inputs from cone penetration tests (CPT), which have been performed across Alameda (U.S. Geological Survey, 2002). The ground shaking is characterized by magnitude and pga, utilizing the 2423 simulations of ground shaking. Depth to groundwater is obtained from the Coastal Storm Modeling System for groundwater levels under sea level rise (Barnard et al., 2019). Using these inputs, LPI is calculated at every CPT location. Artificial fill is expected to exhibit higher liquefaction potential than neighboring, older dune sand (Holzer et al., 2006). CPTs located in dune sand are separated from those in artificial fill based on USGS maps (Witter et al., 2006). Regional analysis is performed on a two-dimensional plane to interpolate LPI values at unknown locations. The regional aspect is performed with sequential Gaussian simulations, characterizing semi-variance versus separation distance with a variogram, treating points within each geologic deposit separately (Fenwick et al., 2014; Mongold and Baker, 2024). The variogram, which defines the spatial correlation structure,

is calculated for each deposit type and each simulation, and values are filled in across the study area based on that variogram. Each simulation produces a different map of LPI across the area. The regional liquefaction hazard simulation is adapted from Mongold and Baker (2024), with some adjustments for computational efficiency. Further details are published in a code repository (See Data availability).

Coastal flooding hazard is adopted from the Adapting to Rising Tides maps (Vandever et al., 2017). Adapting to Rising Tides utilizes a combination of hydrodynamic modeling data and topographic data to determine the flood extents (Vandever et al., 2017). By utilizing these maps, we reconstruct flood hazard curves for Alameda, filling in return periods that are missing for each level of SLR. We find that water depth versus return period (RP) is approximately log-linear, and interpolate using that relationship to obtain water depth values at each location for each missing SLR-RP combination. For depths below known measurements, we fill values of zero to avoid overestimation of risk.

Tsunami hazard is obtained from tsunami hazard maps (State of California, 2023). These probabilistic maps represent return periods of 100, 200, 475, 975, 2475, and 3000 years. These maps include the water depth, which is utilized as the sole parameter to describe the tsunami hazard. Since these maps only represent present-day sea level, we assume a linear increase in water depths with SLR. This is likely an underestimation, as the increase in tsunami depths with SLR will be nonlinear due to wave propagation effects, but past studies have made the same assumption (e.g. Li et al., 2018; Alhamid et al., 2022). Further details on coastal flooding and tsunami hazard modeling under SLR are provided in the Supplementary Information.

3.2 Exposure

The assets of interest are residential buildings in Alameda. Building locations, assessed building values, number of stories, and date of construction, are obtained from the Alameda County Tax Assessor database (Alameda County Assessor's Office, 2021). There is spatial homogeneity of construction year and number of stories of buildings within the city, so missing data are filled in with nearest-neighbor interpolation of nearby buildings. The age of the building is necessary to identify the code level for earthquake ground shaking damage (FEMA, 2020). The number of stories is used within coastal flooding and tsunami vulnerability functions. These exposure data are supplemented with data from the National Structures Inventory which provides first-floor elevations, utilized to determine water depth from the first-floor height (U.S. Army Corps of Engineers, 2024). To align with available vulnerability functions, we limit the inventory to single-family and small construction, at most three stories and four units.

Structural types must also be specified to apply vulnerability functions. Based on national data, probabilities of structural type based on construction year are used to sample these missing data (FEMA, 2002).

We consider a static building stock based on available present-day information, even for the future sea-level-rise analyses.

3.3 Vulnerability

To calculate losses due to ground shaking, Hazus fragility curves are used to sample damage state, DS, of each building given pga. DS is then converted to loss ratio, LR, the repair cost as a fraction of building value (FEMA, 2020). Losses from liquefaction are also calculated using a vulnerability function that relates LPI to LR (Geyin et al., 2020). Since the liquefaction vulnerability function accounts for total loss, from ground shaking and ground failure, the final loss ratio is taken as the maximum of the shaking and liquefaction values.

Flood vulnerability curves developed by Wing et al. (2020) are utilized to obtain loss ratio due to coastal flooding. These curves provide probabilities of different levels of damage, and are sampled for each building and flood scenario to get one simulation of loss. We generate 100 samples of damage for each flood scenario. For the rates of exceeding loss amounts, the flood occurrence rates are divided by the number of samples taken, so that the summation remains the same.

Tsunami vulnerability functions are from Suppasri et al. (2013). These are determined to be the best fit for the case study area as they are calibrated from mostly wood-frame buildings, which make up the majority of buildings in Alameda, and are separated by building height, a known variable for our building stock. Damage states are mapped to loss ratios based on analogous damage state definitions in Goda and De Risi (2017).

Loss is calculated as the LR times the assessed building value for each building. For all hazards, total community loss is the sum of losses to each individual asset. This formulation applies because residential building loss is not a system, but rather a sum of parts. Loss exceedance curves are calculated for each individual hazard as well as for all hazards combined using Eqn. 6. Further details on the vulnerability functions are discussed in the Supplementary Information.

3.4 Risk analysis

The first output that can be considered from the analysis is the building-level present-day average annual loss ratio ($AALR_0$), calculated with Eqn. 2, shown in Fig. 3. The $AALR$ has contributions from all three considered hazards, and highlights the buildings with the highest relative risk. At present, building-level $AALR_{0,k}$ in Alameda range from 0.02-0.045. The largest values are in high-hazard areas on artificial fill soil and low elevations.

The second output is the regional-scale multi-hazard loss, shown under SLR. Fig. 4(a) shows the loss exceedance curves, calculated using Eqn. 6, under present-day and 0.75 m SLR. These results show that the largest impact from SLR comes at regional losses below 1 billion USD. It should be noted that much of this contribution is from frequent coastal flooding events. Without additional adaptation actions, the frequent (including daily high-tide) flooding would cause much of this residential infrastructure to incur repeated damage.

Fig. 4(b) shows how community AAL rises with SLR. AAL, calculated using Eqn. 3, is the area underneath the curves in Fig. 4(a). We can see that losses grow exponentially as sea level increases, from less than 200 million USD in present-day to over 300 million USD with 1 m of SLR and over 600 million USD with 1.5 m of SLR. From Fig. 4(a), this increase in AAL is dominated by the increase in frequent losses below 1 billion USD.

These regional loss metrics can be further disaggregated by the contributing hazard. Fig. 4(a) shows the breakdown of the loss exceedance curves under SLR by contributing hazard.

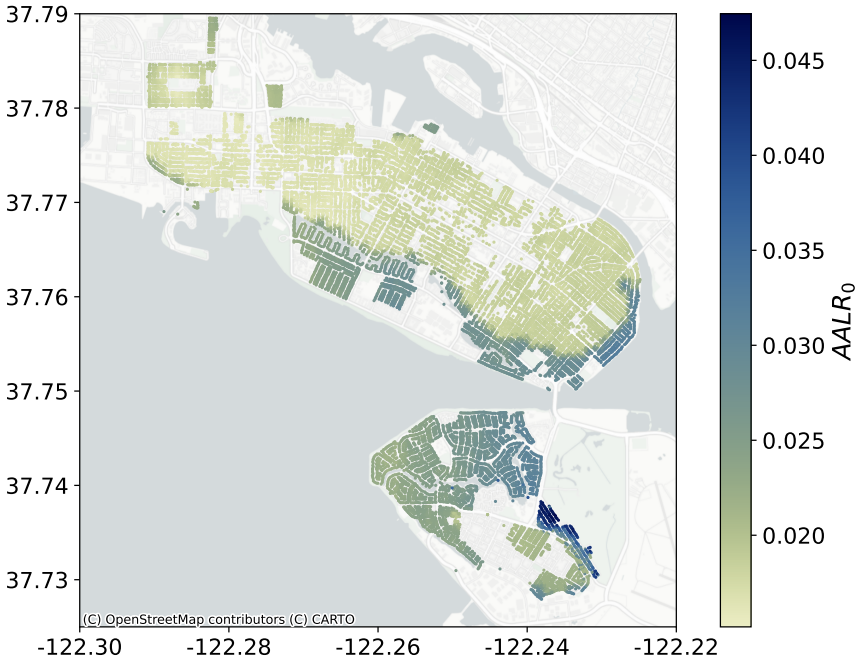

Fig. 3 Present-day building-level average annual loss ratio due to natural hazards.

This plot emphasizes the contribution of the earthquake hazard to the most infrequent and largest losses, and of coastal flooding to the most frequent but smaller losses. The tsunami hazard, in comparison, is infrequent, but also has smaller losses. This finding is due in part to the smaller spatial impact and to the assumed linear increase of inundation with SLR. The hazards' contributions to AAL are shown in different colors in Fig. 4(b). Tsunami barely contributes, while SLR shifts the largest contributor from earthquake, which contributes over 99% of the regional AAL at present-day, to coastal flooding, which is projected to overtake earthquake's contribution at 1.0 m of SLR.

The increase in losses due to SLR, our SLR risk metric defined in Eqn. 5, is shown on a building-level in Fig. 5. Fig. 5(a) shows the increase in $AALR$ under 0.25 m of SLR, and Fig. 5(b) shows the increase in $AALR$ under 0.75 m of SLR. This metric shows the specific building areas most impacted by sea level rise, with respect to loss ratio. The affected areas are low-lying, mostly within artificial fill soil, which is susceptible to liquefaction, and near inland canals and waterways. Thus, these areas should be considered when planning adaptation actions for SLR. These large $AALR$ values come from frequent inundation, indicating that residents likely experience repeated losses over years. These consequence assessments may eventually break down under such frequent events. Damaging events will increasingly to occur during the recovery period following a previous event. The current methodology, which assumes repair costs of buildings in their present state, does not account for impacts from coincident events, or from flood inundation that becomes increasingly permanent.

The timing of sea level rise, as well as the total amount in the far future, has significant uncertainties that cannot be meaningfully reduced (Kopp et al., 2019). Sweet et al. (2022) present five scenarios of San Francisco Bay SLR with a median and 66% confidence interval. These scenarios filter ensemble projections by target values of sea level rise for the end of the century. We obtain the 17th, 50th, and 83rd percentile values directly from the interagency

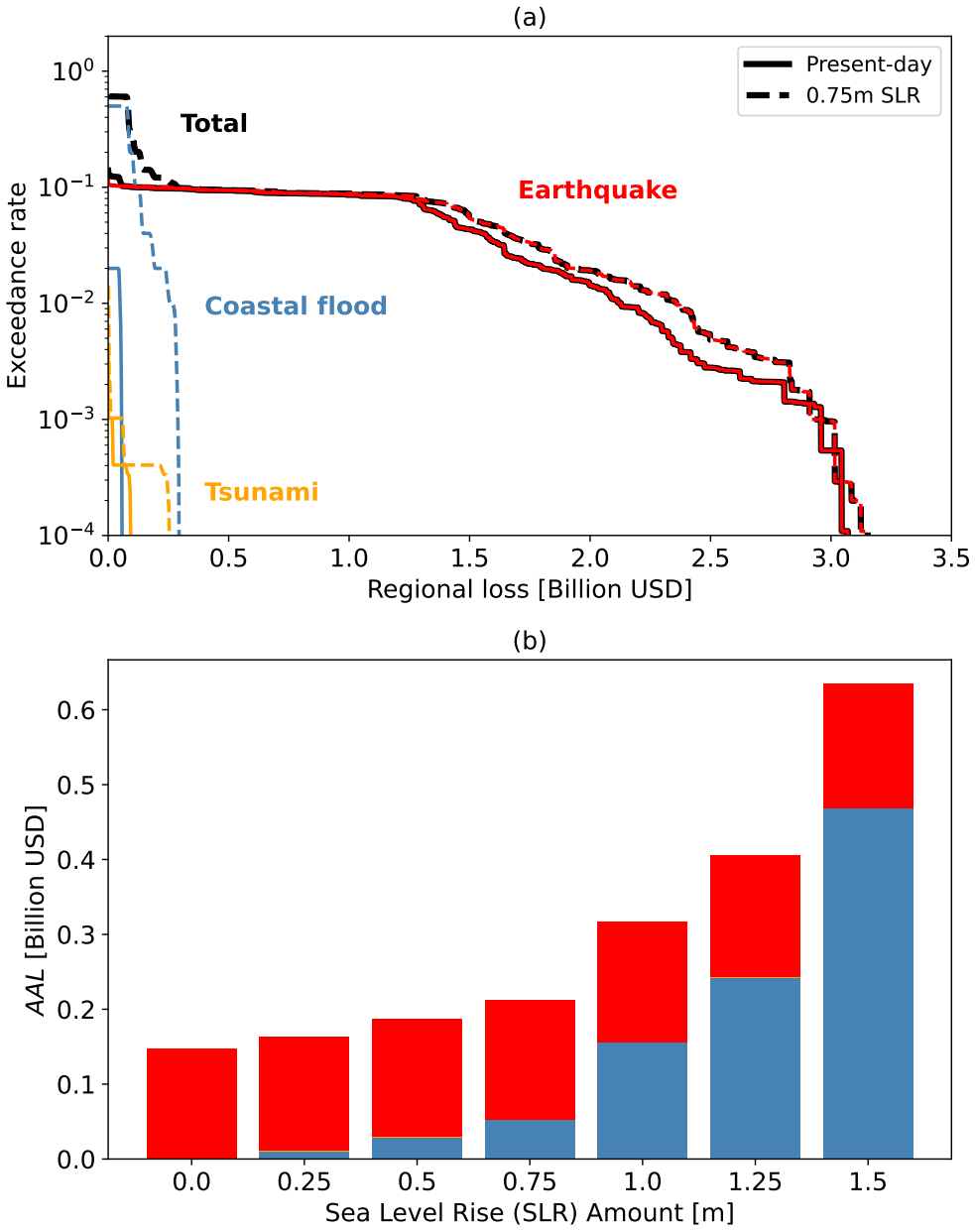

Fig. 4 Loss metrics for total multi-hazard risk under sea level rise shown as (a) loss exceedance curves and (b) average annual loss for levels of SLR, colored by the contribution from each independent hazard pathway.

tool (National Aeronautics and Space Administration (NASA), 2024). In this work, we fit log-normal distributions to the low, intermediate, and high scenarios at each reported time. The log-normal distributions are used to obtain 90% confidence intervals. The log-normal distribution is a good fit to the 17th, 50th, and 83rd percentile values reported for San Francisco, though this may not be generalizable across gauges. Fig. 6(a) shows the probabilistic ranges of SLR until 2100 with 66% and 90% confidence intervals for low, intermediate, and high SLR scenarios.

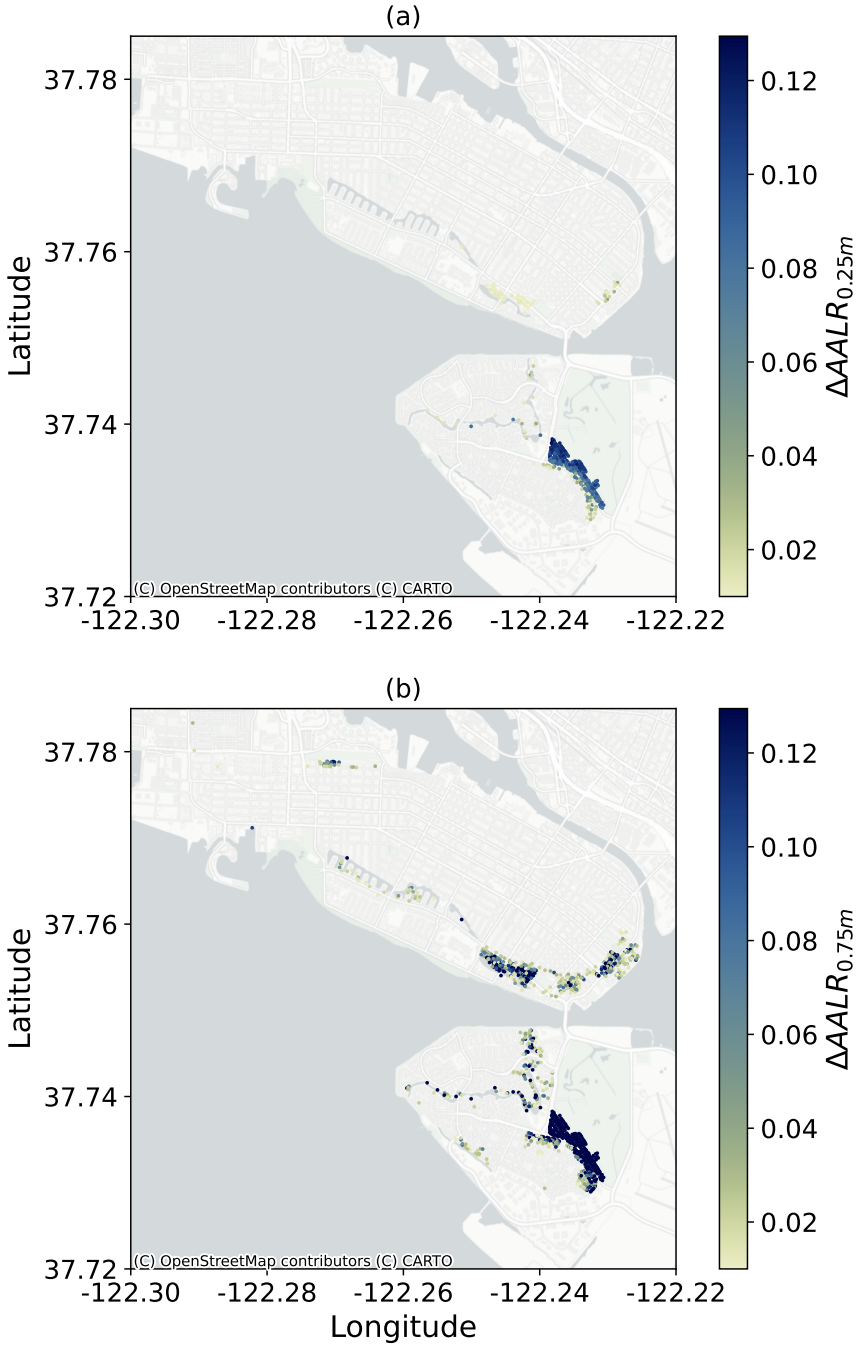

Fig. 5 Change in average annual loss ratio at a building level with (a) 0.25 m and (b) 0.75 m of sea level rise. Buildings are shown that have an increase over 0.01.

We run loss analysis to output the AAL for the confidence intervals of each SLR scenario. Fig 6(b) shows that the projected range spans an order of magnitude by the end of the century.

The horizontal dashed line in Fig. 6(b) shows the total assessed value of all residential buildings in Alameda, 6.95 billion USD. In the high SLR scenario, portfolio losses become a large portion of the portfolio value by the end of the century. Fig. 6(b) emphasizes the

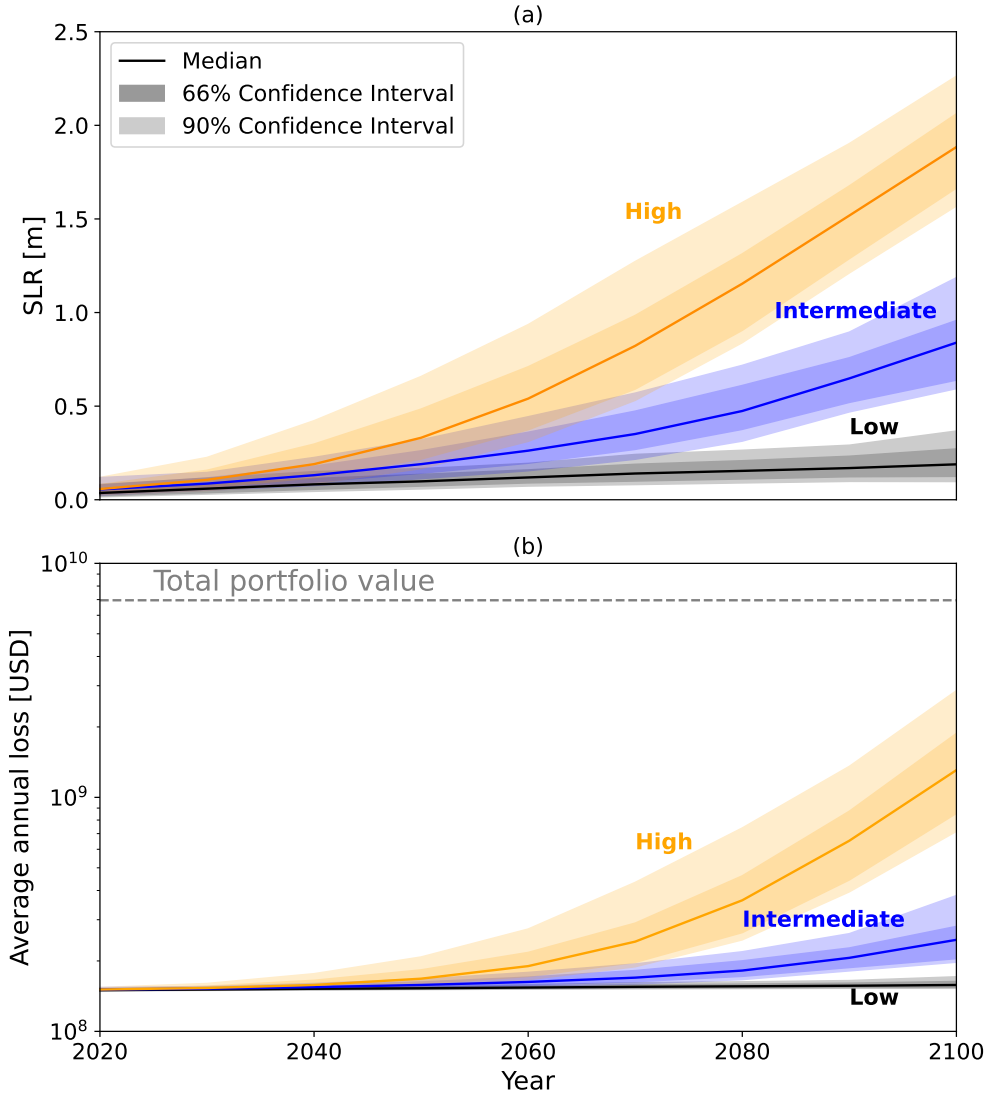

Fig. 6 (a) Local scenarios of SLR over time for San Francisco Bay, using scenario data from (Sweet et al., 2022) and (b) average annual loss of the residential building portfolio of Alameda over time for the three sea level rise scenarios: low, intermediate, and high. Confidence intervals are reported for 66% and 90% confidence. Note that the y-axis is in log scale.

difference between the present-day or low SLR scenario from the high SLR scenario. In any case, actions can be taken now to reduce both present-day risk and avoid frequent and catastrophic losses under SLR by the end of the century.

3.5 Adaptation actions

Three adaptation actions are modeled: managed retreat, raising buildings, and seismic retrofit. While these adaptation strategies are not reflective of specific plans, draft plans could be simulated and compared in this way before implementation. Retrofit ordinances have been implemented in the Bay Area (e.g. City of Alameda, 2024), and FEMA recommends raising houses as a way to reduce flood risk (Federal Emergency Management Agency (FEMA), 2018). Managed retreat has been considered as well in coastal communities, though

precise policies are not modeled here. While exact costs will vary based on the exact policy or program, as well as the specific community, in lieu of a full cost-benefit calculation, approximately same-cost strategies are modeled for a first-pass comparison. Roughly equivalent adaptation costs are proxied by adjusting the portion of buildings affected by each adaptation action, based on anticipated costs of actions per building (Hino et al., 2017; Federal Emergency Management Agency (FEMA), 2018; California Residential Mitigation Program, 2024). Managed retreat is considered for 2% of the building stock, 6% of buildings are assumed to be raised, or 40% of the buildings are assumed to receive a seismic retrofit. These costs are not subtracted from the savings, as they are not precisely known, but the comparisons are informative given their similar costs. For each of the adaptations, buildings are chosen based on either their exposure, vulnerability, or risk. Managed retreat is based on risk, applied to buildings with the highest increase in average annual loss ratios under 0.75 m sea level rise. Alternate metrics, such as average annual loss ratio under present-day or alternate sea level rise conditions prioritized mostly the same buildings and produced roughly equivalent savings, so this choice is not expected to be very sensitive. Raising buildings is based on exposure, prioritizing the buildings with the lowest first floor elevations, considering the land elevation and first floor height. Finally, seismic retrofit is based on vulnerability, with the oldest buildings taking priority, as they have the lowest code level and thus highest seismic vulnerability.

This strategy prioritizes equity, focusing on buildings with the most exposure, vulnerability, or damage ratio rather than the highest dollar loss. Building values across Alameda are similar, however; so this strategy would have more impact in an area with higher socioeconomic disparity. Alternate methods could prioritize the dollar loss values, naturally prioritizing higher value buildings.

Each adaptation action is applied on a building level. Managed retreat is modeled in two ways: by removing the relevant building stock from the portfolio and by replacing the building stock value. These represent upper and lower bounds on the efficacy of relocation policy implementation. Removing the buildings completely captures residents moving to existing vacant buildings within or outside of the considered area. Replacing the building stock assumes that new assets of the same value will take on the average risk of the 98% remaining building stock. The replaced value is modeled by increasing the remaining building stock value. Likely, managed retreat would result somewhere in between, where some new risk is taken on at a lower risk than the average (i.e. new construction outside of liquefaction and flood zones), and some relocation is absorbed into existing buildings. The selected buildings, shown in Fig. 7(a), are prioritized by the change in average annual loss ratio with 0.75 m of SLR, $\Delta AALR_{0.75m}$ (increase in annual risk), which comes from results of Eqn. 5. This metric is chosen as it is how we define annualized climate risk, in this case annual sea level rise risk. Raised houses (Fig. 7(b)) are modeled by increasing the first-floor elevation, which reduces impact from flooding and tsunami, as the inundation depths must be higher before they impact the buildings. For comparison, buildings are raised 1 foot (0.30 m) or 3 feet (0.91 m). While raising houses could have adverse effects on seismic susceptibility if not carefully designed, this trade-off is not quantified in this analysis due to lack of vulnerability data. Seismic retrofit (Fig. 7(c)) of the oldest buildings raises the code level from pre-code

to modern-day high seismic code, reducing damage given the same level of ground shaking. The reduction in shaking losses is applied to the total losses from shaking and liquefaction.

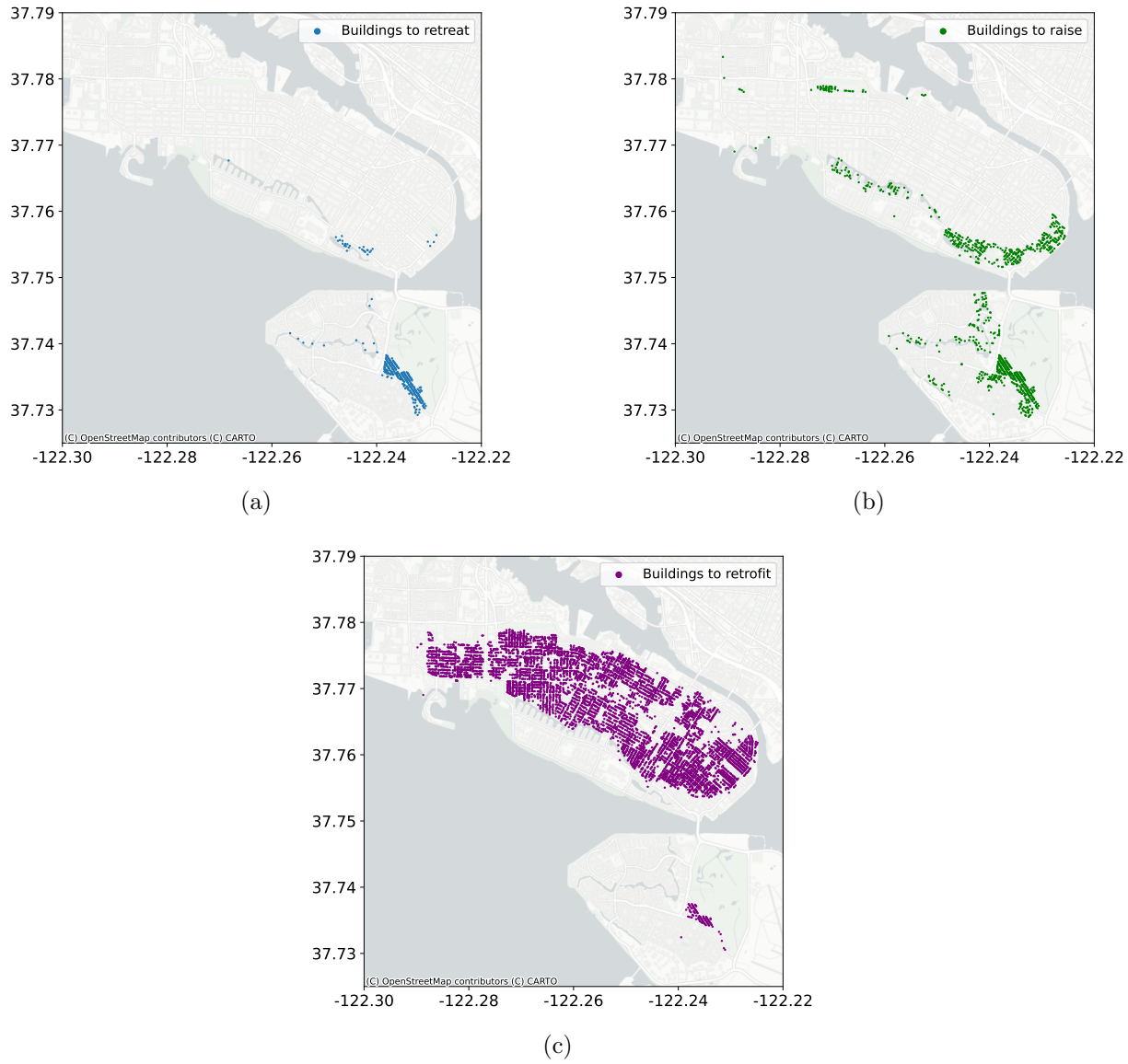

Fig. 7 Building locations affected by each adaptation action: (a) managed retreat, defined as the 2% of buildings with the largest increase in AALR with 0.75m of SLR, (b) buildings to raise, defined as 6% of the building stock with the lowest elevation at the first floor, and (c) seismic retrofit, defined as the oldest 40% of buildings.

The adaptation action's efficacy is measured by the reduction in AAL between baseline and adaptation cases. Through this metric, the benefit of each adaptation action can be compared over multiple levels of SLR, considering all three hazards of interest.

Fig. 8 shows the savings from the adaptation actions for different return period losses. In the present day, shown in Fig. 8(a), retrofit and retreat are relatively close in their reduction of AAL, while raising houses has a lower reduction, as present-day coastal flooding risk is

low. However, under 0.75 m SLR, shown in Fig. 8(b), the savings in AAL from seismic retrofit remains at the same level, while the impact of others increases. Replacing the retreated buildings reduces the efficacy of retreat, and the range between the two bounds increases with SLR. Under 0.75 m of SLR, raising houses surpasses retreat in its efficacy to reduce AAL. It should be noted that raising houses would be ineffective for frequent flooding such as daily high-tide or permanent inundation, as further issues would arise such as road closures, but these impacts are not quantified in this analysis.

However, AAL can emphasize the contributions of frequent events over those of rare events. Adaptations that minimize rare but extreme consequences may also be of interest to a community. To that end, Fig. 8 shows the decrease in loss at various return periods, calculated using Eqn. 9. The return period is $1/\lambda$, and we show $\Delta c(\lambda)$ for multiple return periods. Return periods are shown up to a maximum of 800 years, as earthquake events exhibit enough stochasticity that there is not a purely increasing risk with sea level rise at longer return periods. The stochasticity in the baseline event case can be seen in Fig. 5(a). Both Fig. 8(a) and (b) show a similar trend, which is representative of all amounts of SLR. At short return periods, managed retreat and raising buildings produce large reductions, which is why they are influential in the AAL. However, at long return periods, retrofitting has the largest effect, reducing losses from rare but highly destructive earthquakes. Retreated buildings that reduce the building stock also lower long return period losses, though this benefit is lost almost entirely if the buildings are replaced and assume the average remaining risk. To retain savings, managed retreat programs would need to ensure that new risk is not taken on in the liquefaction and flood zones. Naturally, new construction would have lower risk than older building stock to ground shaking.

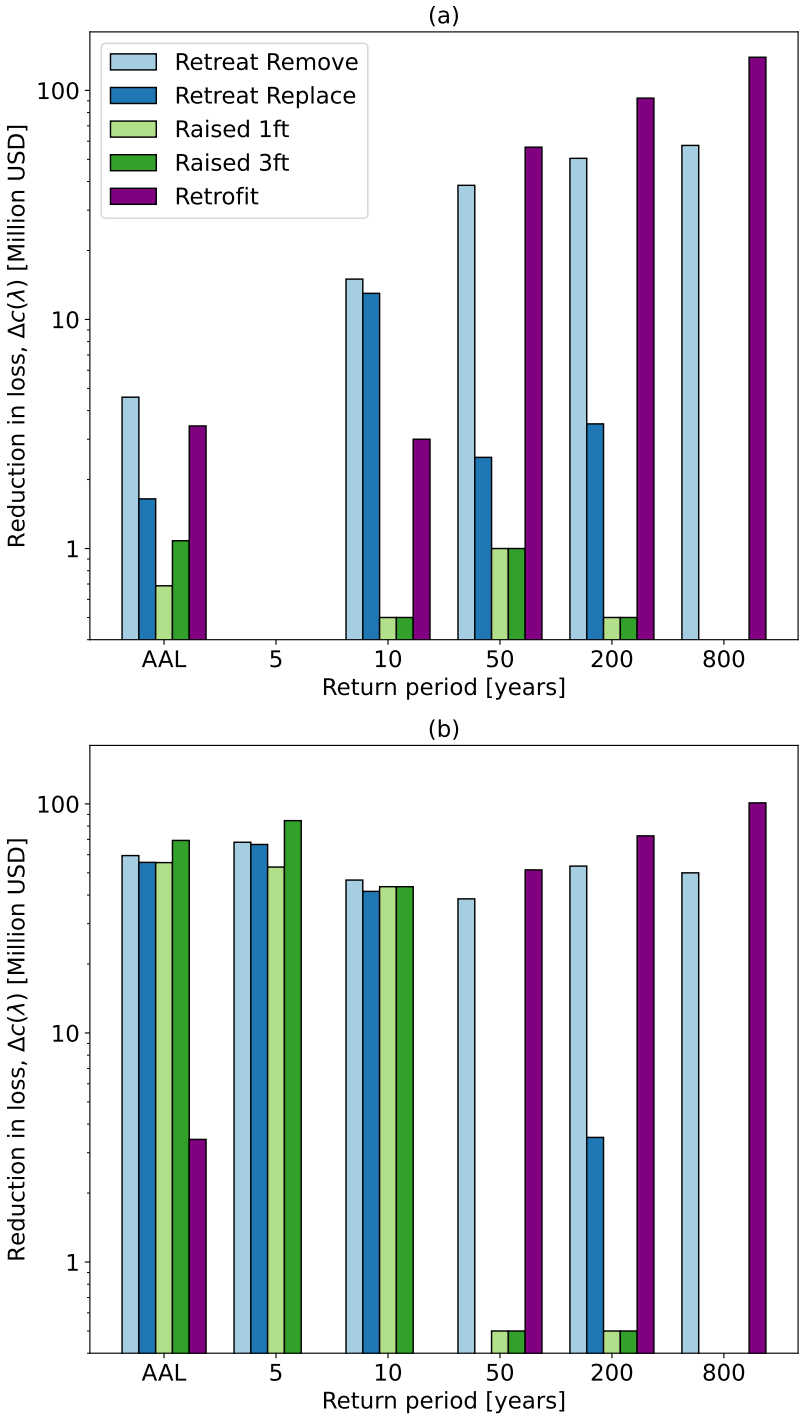

Fig. 8 Reduction in losses for AAL and at different return periods for each adaptation action, from a baseline of no adaptation action. Results are shown for (a) present-day and (b) 0.75 m of SLR. Note that the y-axis is in log-scale.

4 Conclusions

This article presents a methodology to quantify climate change risk at a community scale. The proposed methodology is a risk-based framework, defining climate change risk as the increase in community multi-hazard risk. The methodology combines probabilistic hazard and risk assessment of multiple independent hazard pathways under present-day and future climate conditions. This framework can be applied to different assets, hazards and measures of climate change impact. This methodology can also compare benefits between adaptation actions to inform communities of trade-offs between hazard frequency, climate impacts, and individual hazard losses. This work fills the existing gaps of asset-level multi-hazard analysis under climate change, with the ability to inform community decision-making on adaptation actions.

The proposed methodology is demonstrated on a case study of residential buildings in Alameda, California, under sea level rise (SLR). Alameda is subjected to three independent hazard pathways: earthquake (including ground shaking and liquefaction ground failure), coastal flooding, and tsunami. We find that earthquake hazard dominates the AAL at present-day, but under SLR, the highest contribution changes to coastal flooding. Utilizing SLR scenarios, we demonstrate the wide uncertainty in future natural hazard risk. Finally, a comparison of adaptation actions shows that at present, managed retreat and seismic retrofit may have the highest benefit, but raising buildings would reduce more risk under larger SLR amounts. In addition, seismic retrofit of the oldest buildings is the best adaptation for rare high-impact events. Therefore, it is important to look at both rare and frequent events to understand and manage community risk. The range of potential savings with managed retreat is wide, depending on how a program would be implemented.

Communities facing increasing risk from natural hazards and climate change must make decisions in a multi-hazard, future climate context, considering the benefits of adaptations and the uncertainty of future conditions. Frequent events will dominate risk in some locations; the proposed approach can facilitate the comparison of diverse adaptation actions such as hardening existing assets or retreating for both frequent and rare events. The presented method can be applied to consider different communities, assets, hazards, and climate conditions. To best allocate limited resources, benefits of adaptation actions for different hazards are compared side-by-side in their reduction of present-day and future risk.

Supplementary information. Supplementary information is provided in PDF format.

Acknowledgements. We thank Jaelen Sobers for her work and contributions to the code for the first iteration of sea level rise and liquefaction analysis. We thank Adam Zsarnóczay for his feedback and assistance with the building inventory. We thank Hong Kie Thio for help with tsunami data. We also thank Danielle Mieler, Carmine Galasso, Sarah Fletcher, Neetesh Sharma, Katy Serafin, Corinne Bowers, Jenny Suckale, and Andronikos Skiadopoulos for helpful discussions and feedback.

Some of the computing for this project was performed on the Sherlock cluster. We thank Stanford University and the Stanford Research Computing Center for providing computational resources and support that contributed to these research results.

Declarations

Funding

This work was supported by the National Science Foundation under award numbers DGE-1656518 and CMMI-2053014.

Competing interests

The authors have no relevant financial or non-financial interests to disclose.

Data availability

The datasets generated and/or analyzed during the current study are available at https://doi.org/10.5281/zenodo.13994340.

References

Alhamid, A.K., Akiyama, M., Ishibashi, H., Aoki, K., Koshimura, S., Frangopol, D.M.: Framework for probabilistic tsunami hazard assessment considering the effects of sea-level rise due to climate change. Structural Safety **94**, 102152 (2022)

Alameda County Assessor's Office: Alameda County Parcel Viewer. https://www.acassessor.org/homeowners/assessment-resources/parcel-viewer/

Al-Mutairi, N., Alsahli, M., El-Gammal, M., Ibrahim, M., Abou Samra, R.: Environmental and economic impacts of rising sea levels: A case study in Kuwait's coastal zone. Ocean & Coastal Management **205**, 105572 (2021)

Anthoff, D., Nicholls, R.J., Tol, R.S.: The economic impact of substantial sea-level rise. Mitigation and Adaptation Strategies for Global Change **15**, 321–335 (2010)

Abrahamson, N.A., Silva, W.J., Kamai, R.: Summary of the ask14 ground motion relation for active crustal regions. Earthquake Spectra **30**(3), 1025–1055 (2014) https://doi.org/10.1193/070913EQS198M

Befus, K., Barnard, P.L., Hoover, D.J., Finzi Hart, J., Voss, C.I.: Increasing threat of coastal groundwater hazards from sea-level rise in California. Nature Climate Change **10**(10), 946–952 (2020)

Ballesteros, C., Esteves, L.S.: Integrated assessment of coastal exposure and social vulnerability to coastal hazards in East Africa. Estuaries and Coasts **44**(8), 2056–2072 (2021)

Boruff, B.J., Emrich, C., Cutter, S.L.: Erosion hazard vulnerability of US coastal counties. Journal of Coastal research **21**(5), 932–942 (2005)

Barnard, P.L., Erikson, L.H., Foxgrover, A.C., Finzi Hart, J.A., Limber, P., O'Neill, A.C., Ormondt, M., Vitousek, S., Wood, N., Hayden, M.K., Jones, J.M.: Dynamic flood modeling

essential to assess the coastal impacts of climate change. Scientific Reports **9**, 4309 (2019) https://doi.org/10.1038/s41598-019-40742-z . 13 pages

Bell, R., Glade, T.: Multi-hazard analysis in natural risk assessments. Landslides **1**, 1–10 (2012)

Boulanger, R.W., Idriss, I.M.: Liquefaction susceptibility criteria for silts and clays. Journal of Geotechnical and Geoenvironmental Engineering **132**(11), 1413–1426 (2014) https://doi.org/10.1061/(ASCE)1090-0241(2006)132:11(1413)

Baker, J.W., Jayaram, N.: Correlation of spectral acceleration values from nga ground motion models. Earthquake Spectra **24**(1), 299–317 (2008)

Buchanan, M.K., Kopp, R.E., Oppenheimer, M., Tebaldi, C.: Allowances for evolving coastal flood risk under uncertain local sea-level rise. Climatic Change **137**, 347–362 (2016)

Bosserelle, A.L., Morgan, L.K., Hughes, M.W.: Groundwater rise and associated flooding in coastal settlements due to sea-level rise: a review of processes and methods. Earth's Future **10**(7), 2021–002580 (2022)

Bosello, F., Nicholls, R.J., Richards, J., Roson, R., Tol, R.S.: Economic impacts of climate change in Europe: sea-level rise. Climatic change **112**, 63–81 (2012)

Boore, D.M., Stewart, J.P., Seyhan, E., Atkinson, G.M.: NGA-West2 Equations for Predicting PGA, PGV, and 5% Damped PSA for Shallow Crustal Earthquakes. Earthquake Spectra **30**(3), 1057–1085 (2014) https://doi.org/10.1193/070113EQS184M

California Residential Mitigation Program: Earthquake Brace + Bolt Retrofit. Accessed: 2024-07-23. https://www.californiaresidentialmitigationprogram.com/our-seismic-retrofit-programs/the-retrofits/ebb-retrofit

City of Alameda: Climate action and resiliency plan. Climate action plan, City of Alameda, Alameda, California (September 2019). Accessed: 12 June 2024. https://www.alamedaca.gov/files/sharedassets/public/v/1/public-works/climate-action-page/new-folder/final-carp-9-2019/alameda_carp_final_091119noappendices.pdf

City of Alameda: Earthquake Soft-Story Homeowner Registration is Now Open. Accessed: 2025-02-19 (2024). https://www.alamedaca.gov/Departments/Planning-Building-and-Transportation/Permit-Center/ESS-Homeowner-Registration-is-Now-Open

Cornell, C.A.: Engineering seismic risk analysis. Bulletin of the seismological society of America **58**(5), 1583–1606 (1968)

Chiou, B.S.-J., Youngs, R.R.: Update of the Chiou and Youngs NGA Model for the Average Horizontal Component of Peak Ground Motion and Response Spectra. Earthquake Spectra **30**(3), 1117–1153 (2014) https://doi.org/10.1193/072813EQS219M

De Angeli, S., Malamud, B.D., Rossi, L., Taylor, F.E., Trasforini, E., Rudari, R.: A multi-hazard framework for spatial-temporal impact analysis. International Journal of Disaster Risk Reduction **73**, 102829 (2022)

Depsky, N., Bolliger, I., Allen, D., Choi, J.H., Delgado, M., Greenstone, M., Hamidi, A., Houser, T., Kopp, R.E., Hsiang, S.: Dscim-coastal v1. 1: an open-source modeling platform for global impacts of sea level rise. Geoscientific Model Development **16**(14), 4331–4366 (2023)

Dura, T., Garner, A.J., Weiss, R., Kopp, R.E., Engelhart, S.E., Witter, R.C., Briggs, R.W., Mueller, C.S., Nelson, A.R., Horton, B.P.: Changing impacts of alaska-aleutian subduction zone tsunamis in california under future sea-level rise. Nature communications **12**(1), 7119 (2021)

Diaz, D.B.: Estimating global damages from sea level rise with the Coastal Impact and Adaptation Model (CIAM). Climatic Change **137**(1), 143–156 (2016)

Dunant, A., Robinson, T.R., Densmore, A.L., Rosser, N.J., Rajbhandari, R.M., Kincey, M., Li, S., Awasthi, P.R., Vries, M., Guragain, R., *et al.*: Impacts from cascading multi-hazards using hypergraphs: a case study from the 2015 Gorkha earthquake in Nepal. Natural Hazards and Earth System Sciences **25**(1), 267–285 (2025)

Darwin, R.F., Tol, R.S.: Estimates of the economic effects of sea level rise. Environmental and Resource Economics **19**, 113–129 (2001)

Federal Emergency Management Agency (FEMA): Elevating Your Home? What You Need to Know and Do. Accessed: 2024-07-23. https://www.fema.gov/press-release/20230425/elevating-your-home-what-you-need-know-and-do

FEMA: Hazus-MH 2.1 Technical Manual. Department of Homeland Security, Federal Emergency Management Agency, Washington, D.C. (2002). Department of Homeland Security, Federal Emergency Management Agency

FEMA: Hazus Earthquake Model Technical Manual. Federal Emergency Management Agency, (2020). Federal Emergency Management Agency

Forzieri, G., Feyen, L., Russo, S., Vousdoukas, M., Alfieri, L., Outten, S., Migliavacca, M., Bianchi, A., Rojas, R., Cid, A.: Multi-hazard assessment in Europe under climate change. Climatic Change **137**, 105–119 (2016)

Field, E.H., Jordan, T.H., Cornell, C.A.: OpenSHA: A developing community-modeling environment for seismic hazard analysis. Seismological Research Letters **74**(4), 406–419 (2003)

Felsenstein, D., Lichter, M.: Social and economic vulnerability of coastal communities to sea-level rise and extreme flooding. Natural hazards **71**, 463–491 (2014)

Fenwick, D., Scheidt, C., Caers, J.: Quantifying asymmetric parameter interactions in sensitivity analysis: Application to reservoir modeling. Mathematical Geosciences **46**(4), 493–511 (2014) https://doi.org/10.1007/s11004-014-9530-5

Goda, K., De Risi, R.: Probabilistic tsunami loss estimation methodology: Stochastic earthquake scenario approach. Earthquake spectra **33**(4), 1301–1323 (2017)

Goldwyn, B., Javernick-Will, A., Liel, A.: Dilemma of the tropics: Changes to housing safety perceptions, preferences, and priorities in multihazard environments. Natural Hazards Review **22**(3), 04021012 (2021)

Gill, J.C., Malamud, B.D.: Reviewing and visualizing the interactions of natural hazards. Reviews of geophysics **52**(4), 680–722 (2014)

Geyin, M., Maurer, B.W.: Fragility functions for liquefaction-induced ground failure. Journal of Geotechnical and Geoenvironmental Engineering **146**(12), 04020142 (2020) https://doi.org/10.1061/(ASCE)GT.1943-5606.0002416

Geyin, M., Maurer, B.W., Ballegooy, S.: Lifecycle liquefaction hazard assessment and mitigation. In: Geo-Congress 2020, pp. 312–320 (2020). Reston, VA:American Society of Civil Engineers

Gornitz, V.: Global coastal hazards from future sea level rise. Palaeogeography, Palaeoclimatology, Palaeoecology **89**(4), 379–398 (1991)

Grant, A.R., Wein, A.M., Befus, K.M., Hart, J.F., Frame, M.T., Volentine, R., Barnard, P., Knudsen, K.L.: Changes in liquefaction severity in the San Francisco Bay area with sea-level rise. In: Geo-Extreme 2021, pp. 308–317 (2021)

Holzer, T.L., Bennett, M.J., Noce, T.E., Padovani, A.C., Tinsley III, J.C.: Liquefaction hazard mapping with LPI in the greater Oakland, California, area. Earthquake Spectra **22**(3), 693–708 (2006)

Hino, M., Field, C.B., Mach, K.J.: Managed retreat as a response to natural hazard risk. Nature climate change **7**(5), 364–370 (2017)

Hadipour, V., Vafaie, F., Deilami, K.: Coastal flooding risk assessment using a gis-based spatial multi-criteria decision analysis approach. Water **12**(9), 2379 (2020)

Iannacone, L., Otárola, K., Gentile, R., Galasso, C.: Simulating multi-hazard event sets for life cycle consequence analysis. Natural Hazards and Earth System Sciences **24**(5), 1721–1740 (2024)

Iwasaki, T., Tatsuoka, F., Tokida, K., Yasuda, S.: A practical method for assessing soil liquefaction potential. In: Proceedings of the Second International Conference on Microzonation for Safer Construction, Research, and Application, pp. 885–896 (1978)

Kopp, R.E., Gilmore, E.A., Little, C.M., Lorenzo-Trueba, J., Ramenzoni, V.C., Sweet, W.V.: Usable science for managing the risks of sea-level rise. Earth's future **7**(12), 1235–1269 (2019)

Kwag, S., Ha, J.G., Kim, M.K., Kim, J.H.: Development of efficient external multi-hazard risk quantification methodology for nuclear facilities. Energies **12**(20), 3925 (2019)

Kappes, M.S., Keiler, M., Elverfeldt, K., Glade, T.: Challenges of analyzing multi-hazard risk: a review. Natural hazards **64**, 1925–1958 (2012)

Kafi, K.M., Ponrahono, Z., Salisu Barau, A.: Addressing knowledge gaps on emerging issues in weather and climate extreme events: a systematic review. Climatic Change **177**(3), 56 (2024)

Leatherman, S.P.: Chapter 8 Social and economic costs of sea level rise. In: Douglas, B.C., Kearney, M.S., Leatherman, S.P. (eds.) Sea Level Rise. International Geophysics, vol. 75, pp. 181–223. Academic Press, (2001)

Lung, T., Lavalle, C., Hiederer, R., Dosio, A., Bouwer, L.M.: A multi-hazard regional level impact assessment for Europe combining indicators of climatic and non-climatic change. Global Environmental Change **23**(2), 522–536 (2013)

Laurien, F., Martin, J.G., Mehryar, S.: Climate and disaster resilience measurement: Persistent gaps in multiple hazards, methods, and practicability. Climate Risk Management **37**, 100443 (2022)

Liu, B., Siu, Y.L., Mitchell, G.: Hazard interaction analysis for multi-hazard risk assessment: a systematic classification based on hazard-forming environment. Natural Hazards and Earth System Sciences **16**(2), 629–642 (2016) https://doi.org/10.5194/nhess-16-629-2016

Li, L., Switzer, A.D., Wang, Y., Chan, C.-H., Qiu, Q., Weiss, R.: A modest 0.5-m rise in sea level will double the tsunami hazard in Macau. Science advances **4**(8), 1180 (2018)

Leatherman, S.P., Zhang, K., Douglas, B.C.: Sea level rise shown to drive coastal erosion. Eos, Transactions American Geophysical Union **81**(6), 55–57 (2000)

Mongold, E., Baker, J.W.: Probabilistic regional liquefaction hazard and risk analysis: a case study of residential buildings in Alameda, California. Natural Hazards Review **25**(4), 04024039 (2024)

Mousavi, M.E., Irish, J.L., Frey, A.E., Olivera, F., Edge, B.L.: Global warming and hurricanes: the potential impact of hurricane intensification and sea level rise on coastal flooding. Climatic Change **104**, 575–597 (2011)

Martyr-Koller, R., Thomas, A., Schleussner, C.-F., Nauels, A., Lissner, T.: Loss and damage implications of sea-level rise on small island developing states. Current Opinion in Environmental Sustainability **50**, 245–259 (2021)

Morrison, J.E., Smith, J.A.: Stochastic modeling of flood peaks using the generalized extreme value distribution. Water resources research **38**(12), 41–1 (2002)

Moss, R.E.S., Seed, R.B., Kayen, R.E., Stewart, J.P., Der Kiureghian, A., Cetin, K.O.: CPT-based probabilistic and deterministic assessment of in situ seismic soil liquefaction potential. J. Geotech. Goenviron. Eng. **132**(8), 1032–1051 (2006) https://doi.org/10.1061/(ASCE)1090-0241(2006)132:8(1032)

Ming, X., Xu, W., Li, Y., Du, J., Liu, B., Shi, P.: Quantitative multi-hazard risk assessment with vulnerability surface and hazard joint return period. Stochastic environmental research and risk assessment **29**, 35–44 (2015)

National Aeronautics and Space Administration (NASA): Interagency Sea Level Rise Scenario Tool. Accessed: 2024-06-04 (2024). https://sealevel.nasa.gov/task-force-scenario-tool?psmsl_id=437

Otárola, K., Iannacone, L., Gentile, R., Galasso, C.: Multi-hazard life-cycle consequence analysis of deteriorating engineering systems. Structural Safety **111**, 102515 (2024)

Opabola, E.A.: Simulating multihazard interactions using higher-order network analysis. Natural Hazards Review **25**(4), 04024040 (2024)

Prime, T., Brown, J.M., Plater, A.J.: Physical and economic impacts of sea-level rise and low probability flooding events on coastal communities. PLoS One **10**(2), 0117030 (2015)

Park, H., Cox, D.T., Barbosa, A.R.: Probabilistic Tsunami Hazard Assessment (PTHA) for resilience assessment of a coastal community. Natural Hazards **94**, 1117–1139 (2018)

Reisinger, A., Cammarano, D., Fischlin, A., Fuglestvedt, J.S., Hansen, G., Jung, Y., Ludden, C., Masson-Delmotte, V., Matthews, R., Mintenbeck, J.B.K., Orendain, D.J., Pirani, A., Poloczanskaa, E., Romero, J., Lee, H., Romero, J. (eds.): Annex I: Glossary, pp. 119–130. IPCC, Geneva, Switzerland (2023). https://doi.org/10.59327/IPCC/AR6-9789291691647.002

Shepard, C.C., Agostini, V.N., Gilmer, B., Allen, T., Stone, J., Brooks, W., Beck, M.W.: Assessing future risk: quantifying the effects of sea level rise on storm surge risk for the southern shores of long island, new york. Natural hazards **60**, 727–745 (2012)

Smits, W.K., Attoh, E.M., Ludwig, F.: Flood risk assessment and adaptation under changing climate for the agricultural system in the ghanaian white volta basin. Climatic Change **177**(3), 39 (2024)

Skilodimou, H.D., Bathrellos, G.D., Chousianitis, K., Youssef, A.M., Pradhan, B.: Multi-hazard assessment modeling via multi-criteria analysis and GIS: a case study. Environmental Earth Sciences **78**, 1–21 (2019)

Sanderson, D., Cox, D., Barbosa, A.R., Bolte, J.: Modeling regional and local resilience of

infrastructure networks following disruptions from natural hazards. Journal of Infrastructure Systems **28**(3), 04022021 (2022)

Selva, J.: Long-term multi-risk assessment: statistical treatment of interaction among risks. Natural hazards **67**, 701–722 (2013)

Sharma, N.: Pypsha. https://github.com/neetesh-nks/pypsha

Schlumberger, J., Haasnoot, M., Aerts, J.C., Bril, V., Weide, L., Ruiter, M.: Evaluating adaptation pathways in a complex multi-risk system. Earth's Future **12**(5), 2023–004288 (2024)

Sweet, W.V., Hamlington, B.D., Kopp, R.E., Weaver, C.P., Barnard, P.L., Bekaert, D., Brooks, W., Craghan, M., Dusek, G., Frederikse, T., Garner, G., Genz, A.S., Krasting, J.P., Larour, E., Marcy, D., Marra, J.J., Obeysekera, J., Osler, M., Pendleton, M., Roman, D., Schmied, L., Veatch, W., White, K.D., Zuzak, C.: Global and regional sea level rise scenarios for the united states: Updated mean projections and extreme water level probabilities along u.s. coastlines. Noaa technical report nos 01, National Oceanic and Atmospheric Administration, National Ocean Service, Silver Spring, MD (2022). Accessed: 2024-06-04. https://oceanservice.noaa.gov/hazards/sealevelrise/noaa-nos-techrpt01-global-regional-SLR-scenarios-US.pdf

Sepúlveda, I., Haase, J.S., Liu, P.L.-F., Grigoriu, M., Winckler, P.: Non-stationary probabilistic tsunami hazard assessments incorporating climate-change-driven sea level rise. Earth's Future **9**(6), 2021–002007 (2021)

Suppasri, A., Mas, E., Charvet, I., Gunasekera, R., Imai, K., Fukutani, Y., Abe, Y., Imamura, F.: Building damage characteristics based on surveyed data and fragility curves of the 2011 Great East Japan tsunami. Natural Hazards **66**, 319–341 (2013)

State of California: Probabilistic Tsunami Hazard Analysis Raster Data Version 1, PTHA 18 San Francisco South and PTHA 19 San Francisco. California Geological Survey and AECOM Technical Services; dated 2023, accessed April 19, 2024 (2023)

Turner, R.K., Adger, N., Doktor, P.: Assessing the economic costs of sea level rise. Environment and Planning A **27**(11), 1777–1796 (1995)

Tilloy, A., Malamud, B.D., Winter, H., Joly-Laugel, A.: A review of quantification methodologies for multi-hazard interrelationships. Earth-Science Reviews **196**, 102881 (2019)

U.S. Geological Survey: National Climate Change Viewer (NCCV). Accessed: 2024-09-05. https://apps.usgs.gov/nccv/loca2/nccv2_loca2_watersheds.html

U.S. Geological Survey: Table of CPT Data: Alameda County. https://earthquake.usgs.gov/research/cpt/data/alameda/table/

U.S. Army Corps of Engineers: National Structures Inventory: Technical References. Accessed: 2024-08-06 (2024). https://www.hec.usace.army.mil/confluence/nsi/technicalreferences/latest

Vandever, J., Lightner, M., Kassem, S., Guyenet, J., Mak, M., Bonham-Carter, C.: Adapting to rising tides bay area sea level rise analysis and mapping project. Technical report, Bay Area Toll Authority (2017)

Vlachogiannis, D., Sfetsos, A., Markantonis, I., Politi, N., Karozis, S., Gounaris, N.: Quantifying the occurrence of multi-hazards due to climate change. Applied Sciences **12**(3), 1218 (2022)

Witter, R.C., Knudsen, K.L., Sowers, J.M., Wentworth, C.M., Koehler, R.D., Randolph, C.E., Brooks, S.K., Gans, K.D.: Maps of Quaternary Deposits and Liquefaction Susceptibility in the Central San Francisco Bay Region, California (No. 2006-1037). Technical report, U.S. Geological Survey (2006). https://doi.org/10.3133/ofr20061037

Wing, O.E., Pinter, N., Bates, P.D., Kousky, C.: New insights into us flood vulnerability revealed from flood insurance big data. Nature communications **11**(1), 1444 (2020)

Zscheischler, J., Martius, O., Westra, S., Bevacqua, E., Raymond, C., Horton, R.M., Hurk, B., AghaKouchak, A., Jézéquel, A., Mahecha, M.D., Maraun, D., Ramos, A.M., Ridder, N.N., Thiery, W., Vignotto, E.: A typology of compound weather and climate events. Nature Reviews Earth & Environment **1**(7), 333–347 (2020) https://doi.org/10.1038/s43017-020-0060-z

Zhang, L.M., Zhang, S.: Approaches to multi-hazard landslide risk assessment. In: Geotechnical Safety and Reliability, pp. 312–323 (2017)